analytical chemistry

pubs.acs.org/ac Article

Detection and Characterization of Vesicular Gangliosides Binding to Myelin-Associated Glycoprotein on Supported Lipid Bilayers

Jennie L. Cawley, Luke R. Jordan, and Nathan J. Wittenberg*

Cite This: https://dx.doi.org/10.1021/acs.analchem.0c04412 Read Online

ACCESS | Metrics & More | Article Recommendations | Supporting Information

ABSTRACT: In the nervous system, a myelin sheath that originates from oligodendrocytes or Schwann cells wraps around axons to facilitate electrical signal transduction. The interface between an axon and myelin is maintained by a number of biomolecular interactions. Among the interactions are those between GD1a and GT1b gangliosides on the axon and myelin-associated glycoprotein (MAG) on myelin. Interestingly, these interactions can also inhibit neuronal outgrowth. Ganglioside−MAG interactions are often studied in cellular or animal models where their relative concentrations are not easily controlled or in assays where the gangliosides and MAG are not presented as part of fluid lipid bilayers. Here, we present an approach to characterize MAG−ganglioside interactions in real time, where MAG, GD1a, and GT1b contents are controlled and they are in their in vivo orientation within fluid lipid bilayers. Using a quartz crystal microbalance with dissipation monitoring (QCM-D) biosensor functionalized with a supported lipid bilayer (SLB) and MAG, we detect vesicular GD1a and GT1b binding and determine the interaction kinetics as a function of vesicular ganglioside content. MAG-bound vesicles are deformed similarly, regardless of the ganglioside or its mole fraction. We further demonstrate how MAG−ganglioside interactions can be disrupted by antiganglioside antibodies that override MAG-based neuron growth inhibition.

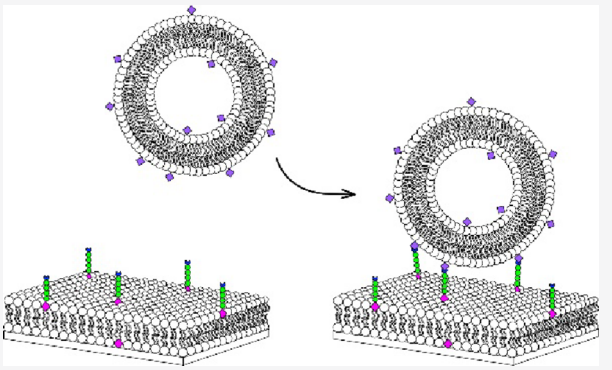

In the nervous system, axons are insulated by myelin sheaths that originate from oligodendrocytes or Schwann cells. The interface between an axon and the myelin sheath, known as the periaxonal space, is a 9−12 nm-wide gap[1] that is home to many molecular interactions crucial for maintaining myelin and axon integrity as well as efficient signal transduction. One example is myelin-associated glycoprotein (MAG) binding to GD1a and GT1b gangliosides and Nogo receptor 1 (NgR1) on the surface of the axon.[2] MAG is a part of a family of proteins known as sialic acid binding immunoglobulin-type lectins (Siglecs), which are transmembrane proteins that bind sialylated molecules and are involved in cellular signaling and adhesion. Unlike other Siglecs, which are primarily involved in immune system function,[3] MAG is exclusively expressed in the nervous system, and it is the only Siglec to be found there.[4] Specifically, MAG is found on the innermost wrap of myelin and is among the proteins responsible for adhering myelin to the axon.[5,6] MAG recognizes sialic acids with an α2,3 linkage, such as those found on the terminal galactose of GD1a and GT1b gangliosides,[7] and ganglioside binding is thought to stabilize MAG dimerization.[5] In nervous system repair, binding of MAG to gangliosides and NgR1 initiates the RhoA signaling cascade in neurons, which ultimately leads to growth cone collapse and inhibition of neurite outgrowth.[8] Therefore, MAG is one of the myelin-associated molecules that present an obstacle to nervous system repair in response to neuro-degenerative diseases or traumatic nervous system injury.[9] A number of studies have shown that inhibiting MAG−ganglioside interactions can result in an enhanced neurite outgrowth in vitro and in animal models of nervous system injury.[10−12]

Previous research on the interactions between MAG and gangliosides have employed a variety of assays including immunoassays, surface plasmon resonance,[5] cellular adhesion assays,[13] and neurite outgrowth assays.[5,10,14] Although these assays have provided valuable insights into MAG−ganglioside interactions, they can suffer from some drawbacks. Specifically, some of these assays lack fluid lipid bilayer membranes for MAG and gangliosides to reside in, the MAG and ganglioside orientations are uncontrolled, and they lack the ability to detect molecular interactions in real time to evaluate kinetics. To overcome these drawbacks, it is desirable to design a biomimetic system where MAG and gangliosides are immobilized with precisely controlled orientations and are

Received: October 19, 2020
Accepted: November 27, 2020

associated with separate but interacting fluid lipid bilayer membranes. Integrating this system into a surface-based biosensor platform can enable binding measurements with temporal resolution sufficient for determining binding kinetics.

Quartz crystal microbalance with dissipation monitoring (QCM-D)[15] is a surface-based sensing technique that can monitor adsorption of molecules or particles on surfaces, including supported lipid bilayer (SLB)-functionalized surfaces, as a function of time.[16−20] Here, we describe a QCM-D-based approach to monitor MAG−ganglioside interactions in real time using a system that mimics the periaxonal space through the use of supported lipid bilayers and vesicles (Figure 1). Our system uses a SiO_2-coated QCM-D chip onto which a

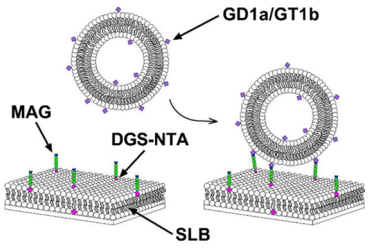

Figure 1. Vesicular gangliosides bind SLB-conjugated MAG. A SLB containing DGS-NTA is formed on a QCM-D sensor chip, and then histidine-tagged MAG is conjugated to the surface (left). Vesicles containing GD1a or GT1b are injected and bind the surface via ganglioside−MAG interactions (right).

SLB is formed. Then, the extracellular domain of MAG with a polyhistidine tag is conjugated to the SLB via lipids with NTA-nickel headgroups. This makes the sensor chip a model of the myelin membrane where the lipids and MAG are diffusionally mobile, and MAG is conjugated to the surface with the proper orientation. Phospholipid vesicles that include gangliosides, to mimic the lipid composition of the axon, are then injected into the flow cell and their binding to the MAG-functionalized surface is detected as a frequency shift in the QCM-D signal. We found that the presence of GD1a or GT1b in the vesicles is required for binding to MAG. Furthermore, vesicle adsorption kinetics depend on the ganglioside mole fraction, and the amount of vesicle deformation upon MAG binding is independent of ganglioside mole fraction. Finally, we show that monoclonal antibodies similar to those that override MAG-based inhibition of neuronal growth can inhibit the binding of GD1a and GT1b to MAG.

EXPERIMENTAL SECTION

Reagents and Chemicals. All vesicles were prepared from the following lipids: 1-palmitoyl-2-oleoyl-glycero-3-phosphocholine (POPC), nickel-loaded 1,2-dioleoyl-sn-glycero-3-[(N-(5-amino-1-carboxypentyl)iminodiacetic acid)succinyl] (DGS-NTA), 1,2-dioleoyl-sn-glycero-3-phosphoethanolamine-N-(7-nitro-2-1,3-benzoxadiazol-4-yl) (NBD-PE), GM1 (ovine brain) (Avanti Polar Lipids, USA), GD1a (bovine brain), GT1b (bovine brain), and GD1b (bovine brain) (Sigma-Aldrich). Bovine serum albumin (BSA) was purchased from Sigma-Aldrich. Histidine-tagged recombinant mouse MAG protein was obtained from Sino Biological. Cholera toxin B subunit (CTB) was purchased from ThermoFisher Scientific. GD1a-1, GT1b-2b, GM1-1a, and GD1b-1s antibodies were purchased from the Developmental Studies Hybridoma Bank at the University of Iowa. Two buffers were used in this work: "Tris1" (10 mM Tris, 150 mM NaCl, pH 7.0) and "Tris3" (10 mM Tris, 150 mM NaCl, 2.2 mM $CaCl_2$, pH 7.0). All buffer chemicals were purchased from Sigma-Aldrich or ThermoFisher Scientific.

Preparation of Lipid Vesicles. Lipids were dissolved in chloroform or a chloroform/methanol mixture at the desired molar ratios and subsequently underwent solvent evaporation under vacuum. The dried lipid films were rehydrated with Tris1 to a concentration of 1 mg/mL, vortexed, and bath sonicated for 10 min prior to extrusion (Mini-Extruder, Avanti Polar Lipids) through a 50 nm pore filter (polycarbonate track etch membranes, Avanti Polar Lipids). Lipids were extruded with 23 passes. Vesicles (POPC/1% DGS-NTA) for SLB formation were diluted to a total lipid concentration of 0.1 mg/mL with Tris3. Vesicles (POPC, POPC/GD1a, and POPC/GT1b) used in MAG binding studies were prepared in Tris1 as described above and then diluted with additional Tris1 to either 0.1, 0.2, or 0.4 mg/mL. Vesicle concentrations were calculated based on the total amount of lipid in a sample (0.1, 0.2, or 0.4 mg/mL), the molecular weight of POPC, the mean vesicle radius from dynamic light scattering (DLS), an area per lipid of 64 $Å^2$, and a 39 Å bilayer thickness.[21]

Formation of SLB on QCM-D Sensor Chip. The apparatus used consisted of a QCM-D (Q-Sense E1 Explorer, Biolin Scientific) utilizing a 5 MHz AT-cut quartz crystal. The SiO_2-coated QCM-D sensor chips were prepared by UV-ozone treatment (ProCleaner Plus, Bioforce Nanosciences), a subsequent soak in 2% (w/v) sodium dodecyl sulfate solution, extensive rinse with DI water, blowing dry with N_2 gas, and a final UV-ozone treatment. The sensor chips were mounted in the QCM-D flow cell, and Tris1 buffer was flowed over them within 5 min. The temperature of the flow cell and the flow rate were held constant at 23.0 °C and 0.1 mL/min, respectively. The injection sequence for supported bilayer formation was Tris1, 0.1 mg/mL vesicles in Tris3, Tris1. Frequency and dissipation were monitored at the 1st, 3rd, 5th, 7th, 9th, and 11th overtones, with all analysis performed using the 3rd overtone. To assess if SLBs were continuous and defect-free, BSA in Tris1 was injected following SLB formation.

Protein Functionalization of SLB. Histidine-tagged MAG with a concentration of 10 nM in Tris1 was flowed over a continuous SLB containing 1% DGS-NTA until a frequency shift of −30 Hz. Injection of the MAG was followed by Tris1 to wash away any unbound protein.

Vesicle Binding Monitored by QCM-D. For ganglioside−MAG binding studies, vesicles with a total lipid concentration ranging from 0.1 to 0.4 mg/mL in Tris1 were injected and followed by Tris1 only. For antiganglioside antibody inhibition studies, vesicles ranging from 0.1 to 0.2 mg/mL were exposed to various concentrations (1−50 nM) of antiganglioside antibodies for 1 h, prior to injection over a functionalized SLB containing histidine-tagged MAG. Injection sequence for antibody inhibition studies was the following: vesicles co-incubated with antiganglioside antibodies in Tris1, Tris1.

Fluorescence Recovery after Photobleaching Measurements. Glass coverslips were cleaned with an aqueous 2% (v/v) Hellmanex III solution at 35 °C, rinsed with ultrapure H_2O, and then dried under N_2 gas. Polydimethylsiloxane (PDMS) elastomer wells were bonded to the coverslips by treatment of both surfaces with a plasma cleaner (Harrick Plasma, Ithaca, NY) using gases at approximately 250 mTorr

https://dx.doi.org/10.1021/acs.analchem.0c04412
Anal. Chem. XXXX, XXX, XXX−XXX

for 1.5 min. Vesicles to form SLBs for microscopy contained either POPC and 1 mol % NBD-PE or POPC with 1.0 mol % NBD-PE and 1 mol % DGS-NTA. The vesicles were diluted to 0.1 mg/mL in Tris3 buffer and were added to the PDMS wells within 10 min, and then incubated for 15 min. After incubation, excess vesicles were removed by washing with Tris1 buffer and immediately imaged using an inverted microscope (Eclipse Ti, Nikon) equipped with a 100× oil immersion objective with a 1.49 numerical aperture. Fluorescence was excited using a LED light engine (Aura II, Lumencor), a FITC filter set (Chroma), and images were captured with a 2048 × 2048 pixel sCMOS camera (Orca Flash 4.0 v2, Hamamatsu). Each sample was photobleached using a 405 nm laser (50 mW) pulse for 2 s, and fluorescence recovery was captured at 1 s intervals for 120 s. After FRAP of the lipid bilayer, 10 nM histidine-tagged MAG was added to the chamber and incubated for 15 min. After incubation, excess MAG was removed by washing, and lipid diffusion was again analyzed via FRAP. Lipid diffusion coefficients and mobile fractions were calculated using the Hankel transform method and MATLAB code described by Jönsson et al.[22] FRAP images were processed using the Fiji ImageJ package.[23]

Dynamic Light Scattering. Vesicle sizes were measured by DLS. An ALV/CGS-3 Compact Goniometer System spectrometer was used to collect DLS measurements in triplicate. Lipid vesicles were diluted to 0.22 mg/mL in Tris1 buffer prior to analysis.

Zeta Potential Measurements. Zeta potential measurements were obtained using a ZetaPALS Zeta Potential Analyzer (Brookhaven Instruments Corp.). Extruded vesicles, prepared with the desired lipid compositions as described above, were diluted to 0.22 mg/mL in 0.01 M NaCl. The temperature was held constant at 25 °C. Data reported are as the mean ± standard deviation for each vesicle composition from a total of 20 measurements per sample.

Statistical Analysis. All curve fitting and analysis were done using the Prism 8, GraphPad software with a minimum of $n = 3$.

RESULTS AND DISCUSSION

Biosensor Functionalization. The first step in creating a biosensor that mimics myelin is to form a SLB on a SiO_2-coated QCM-D sensor chip. To form SLBs, precursor vesicles were first prepared that contained POPC only or POPC with 1% DGS-NTA to conjugate histidine-tagged MAG. All lipid compositions are expressed as mole %. The vesicles were injected into the QCM-D flow cell where they spontaneously ruptured on the SiO_2 surface of the sensor chip (Figure 2a). Both vesicle types resulted in SLBs that had final frequency and dissipation values that are indicative of a continuous uniform membrane film. The POPC SLB had a final frequency shift (ΔF) of −28.3 Hz and a final dissipation shift (ΔD) of 0.55×10^{-6}. These values agree with accepted frequency and dissipation shift ranges for a continuous SLB film.[24,25] The presence of the DGS-NTA resulted in a slightly more negative frequency shift plateau, indicative of a slightly more dense and/or thick SLB (Figure 2a). The formation of a continuous, defect-free SLB was verified by the negligible frequency shift, i.e., mass accumulation, after the injection of BSA over the POPC/DGS-NTA SLB (Figure S1). BSA adsorbs to bare SiO_2,[26] thus the lack of BSA adsorption after SLB formation confirms a defect-free supported lipid bilayer.

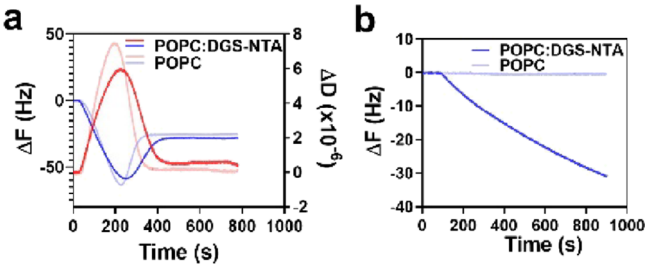

Figure 2. Biosensor functionalization. (a) QCM-D frequency (blue) and dissipation (red) signals show that vesicles composed of POPC alone or POPC/1% DGS-NTA adsorb and spontaneously rupture to form SLBs on SiO_2-coated sensor chips. (b) QCM-D frequency shift showing the conjugation of MAG to a SLB composed of POPC/1% DGS-NTA (dark blue). MAG does not adsorb on to a SLB composed solely of POPC (light blue).

Next histidine-tagged MAG was conjugated to the SLB. The DGS-NTA in the SLB was held at 1%, and MAG was injected until ΔF reached approximately −30 Hz (Figure 2b). After MAG-SLB conjugation, the QCM-D frequency signal remained constant for more than 3 h, confirming the stability of the MAG conjugation to the SLB (Figure S2). There was no detectable conjugation of MAG to the SLB lacking DGS-NTA (Figure 2b). The introduction of imidazole caused the frequency to return to near baseline by displacing MAG (Figure S2). Together, this confirms that the MAG is conjugated to the SLB via the DGS-NTA lipid and the conjugation is stable. Fluorescence recovery after photobleaching (FRAP) experiments show that the SLBs retain fluidity after MAG conjugation (Figures S3 and S4). The conjugation of MAG to the functionalized SLB has very minimal effects on SLB fluidity (Table S1).

Detection of Ganglioside Vesicles Binding to MAG on SLBs. To mimic axon-myelin membrane−membrane interactions, we injected ganglioside-containing vesicles over SLBs with and without conjugated MAG. The fraction of gangliosides in the vesicles ranged from 0 to 4% and the total lipid concentration of the vesicle suspensions ranged from 0.1 to 0.4 mg/mL. Vesicles were characterized by DLS and a zeta potential analyzer. Vesicle diameters were determined by DLS and ranged from 110 to 150 nm (Figure S5a). GD1a and GT1b both possess sialic acid groups and have charges of −2 and −3, respectively. Vesicles containing 4% GT1b yielded the negative largest zeta potential among all vesicles, and zeta potentials became less negative as the ganglioside concentration was decreased, as expected (Figure S5b). Figures 3 and 4 show the frequency shift (plotted as $|\Delta F|$) as a function of time for vesicles containing 1−4% GD1a and GT1b binding to MAG. As vesicles with GD1a or GT1b bound to the MAG-functionalized surface, the dissipation signal increased continuously and then reached a plateau concurrent with the frequency shift (Figure S6). This suggests the vesicles bind to MAG and remain intact rather than rupture.[24] The injection of vesicles was followed by an injection of Tris1 buffer. During the infusion of the buffer, a small fraction of vesicles desorbed in all cases, and the vesicles containing 1% GD1a desorbed the most, as a fraction of their maximum frequency shift. The lack of significant vesicle desorption for most compositions indicates that MAG−ganglioside mediated vesicle−SLB adhesions are mostly permanent, at least under the conditions studied here. The near-permanent nature of these contacts is likely driven by multiple MAG−ganglioside interactions per

https://dx.doi.org/10.1021/acs.analchem.0c04412
Anal. Chem. XXXX, XXX, XXX−XXX

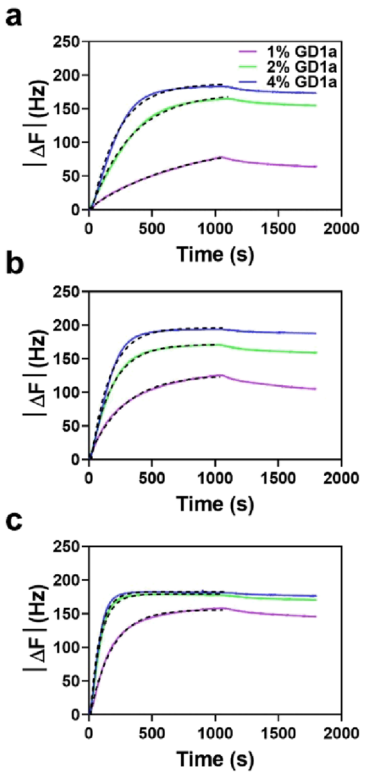

Figure 3. QCM-D detection of vesicles with GD1a binding to MAG-conjugated SLBs. Binding curves showing absolute value of frequency shift, $|\Delta F|$, as a function of time for vesicles containing 1, 2, and 4% GD1a. Total lipid concentrations are (a) 0.1 mg/mL, (b) 0.2 mg/mL, and (c) 0.4 mg/mL. Dashed lines during the association phase are fits to eq 1.

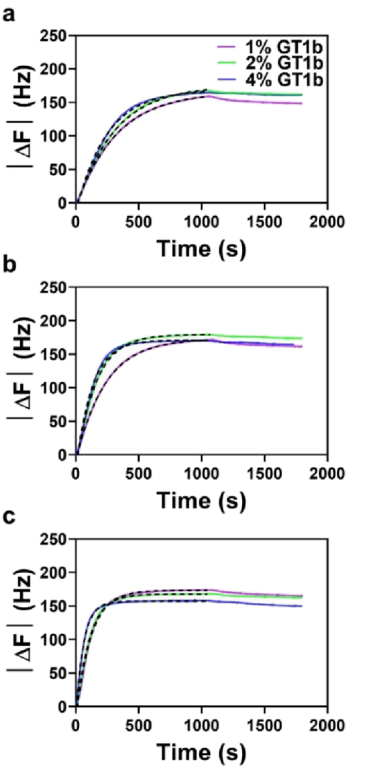

Figure 4. QCM-D detection of vesicles with GT1b binding to MAG-conjugated SLBs. Binding curves showing the absolute value of frequency shift, $|\Delta F|$, as a function of time for vesicles containing 1, 2, and 4% GT1b. Total lipid concentrations are (a) 0.1 mg/mL, (b) 0.2 mg/mL, and (c) 0.4 mg/mL. Dashed lines during the association phase are fits to eq 1.

vesicle. Multivalent particle-surface interactions are well-established as a mechanism for enhanced receptor-mediated particle-surface binding, especially when individual interactions are weak.[27] Vesicles containing 1% GD1a and 1% GT1b were also injected over a POPC/1% DGS-NTA SLB lacking MAG. This resulted in negligible binding, confirming that the binding results presented here are a result of protein−lipid interactions and not lipid−lipid interactions (Figure S7).

Vesicles composed of POPC, POPC with 2% GD1b, and POPC with 2% GM1 do not bind MAG-conjugated SLBs (Figure S8). This confirms MAG's specificity for gangliosides with α2,3-sialic acid linkages, which are found between the sialic acids on the terminal galactose in GD1a and GT1b but are absent in GD1b and GM1. Previously, Collins and coworkers investigated the adherence of Chinese hamster ovary cells and COS-1 kidney fibroblasts transfected to express MAG to substrates coated with various gangliosides. They observed that these cells strongly adhered to substrates with GD1a and GT1b but had significantly lower adherence to substrates with GD1b and GM1.[13] Thus, our SLB−vesicle binding assay recapitulates cellular adhesion studies in a system where ganglioside and MAG content can be tightly controlled.

A quantitative evaluation of the vesicle adsorption kinetics was conducted by fitting the curves to the following equation:

$$|\Delta F| = |\Delta F_{max}|(1 - e^{-t/\tau}) \quad (1)$$

where $|\Delta F|$ is the absolute value of the frequency shift as a function of time, $|\Delta F_{max}|$ is absolute value of the maximum frequency shift, t denotes time, and τ is the characteristic adsorption time.[28] The values of τ decreased as function of ganglioside concentration and were generally smaller for vesicles with GT1b compared to equivalent vesicles with GD1a. The characteristic adsorption time (τ) is inversely proportional to the observed rate constant for vesicle adsorption ($k_{obs} = 1/\tau$), and $k_{obs} = k_a C_v + k_d$, where C_v is the vesicle concentration, and k_a and k_d are the rate constants for association and dissociation, respectively.[29] A plot of $1/\tau$ vs C_v (Figure 5) reveals the vesicle dissociation constant, K_D,

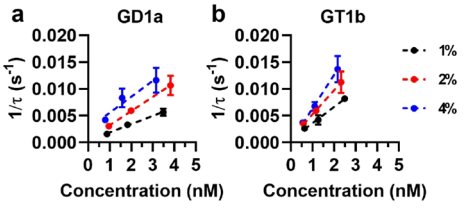

Figure 5. Determination of kinetic constants. The inverse of characteristic adsorption time ($1/\tau$) for (a) GD1a and (b) GT1b vesicle binding plotted as a function of the vesicle concentration.

because $K_D = k_d/k_a$. We calculated K_D values for 1, 2, and 4% GD1a vesicles as $(2.2 \pm 1.8) \times 10^{-10}$ M, $(2.2 \pm 0.6) \times 10^{-10}$ M, and $(8.5 \pm 6.0) \times 10^{-10}$ M, respectively. For 1, 2, and 4% GT1b vesicles, the K_D values were $(1.9 \pm 1.0) \times 10^{-10}$ M, $(1.9 \pm 0.4) \times 10^{-10}$ M, and $(2.3 \pm 0.6) \times 10^{-11}$ M, respectively. A summary of kinetic data is provided in Table S2. Previous MAG−ganglioside binding studies have suggested that GD1a and GT1b bind MAG equivalently;[13] however, no

https://dx.doi.org/10.1021/acs.analchem.0c04412
Anal. Chem. XXXX, XXX, XXX−XXX

estimates of binding constants have appeared in the literature. Qualitatively, our results agree with earlier studies; however, the advantageous use of a real-time biosensor allows us to extract binding kinetics that show the binding rate for GT1b > GD1a. The K_D values we determined indicate high-affinity binding between vesicular gangliosides and SLB-conjugated MAG. The especially tight binding is facilitated by multivalent vesicle−SLB interactions. In fact, the K_D values measured here are over an order of magnitude smaller than for shiga toxin-conjugated lipid particles binding to Gb3 glycolipids in cell membranes.[29]

Vesicle Deformation upon Binding. Vesicles can significantly deform upon adsorption to surfaces,[30] and QCM-D can be used to determine the extent of deformation.[31] The interplay between adhesion and bending energies governs vesicle adsorption and subsequent deformation.[32] While our dissipation data suggest that vesicles with GD1a or GT1b do not rupture upon binding to MAG-functionalized SLBs (Figure S6), we sought to determine if their ganglioside content effected the extent of deformation by plotting ΔD vs ΔF. The more vesicles are deformed upon adsorption, the less energy they will dissipate because a more deformed vesicle layer is more tightly coupled to the surface and thus has lower viscoelasticity. In plots of ΔD vs ΔF for vesicular adsorption, a larger slope is indicative of a less deformed (more viscoelastic) vesicular layer. Other groups have utilized this approach to determine the extent of adsorbed vesicle deformation and/or rupture[33] or the relative rigidity of an adsorbed layer of virions bound to glycosphingolipid containing SLBs.[34]

For a given ganglioside concentration, the slopes for GD1a and GT1b are not significantly different (Figure 6). This suggests that GT1b and GD1a vesicles bind MAG with a similar adhesive strength and there are no significant differences in vesicle deformation between GT1b and GD1a vesicles possessing the same ganglioside mole fraction. As the ganglioside mole fraction varies, the slopes of the plots for GD1a and GT1b do not significantly change, which means that there is no significant difference in vesicle deformation as a function of ganglioside surface coverage. For comparison, the plots of ΔD vs ΔF for the adsorption of these vesicles on SiO_2 have significantly lower slopes (Figure 6), which indicates that the vesicles deform significantly more on SiO_2 than they do on MAG-functionalized SLBs. We expect vesicles with these compositions to significantly deform on SiO_2 surfaces because they will eventually rupture to form a SLB on SiO_2.[35]

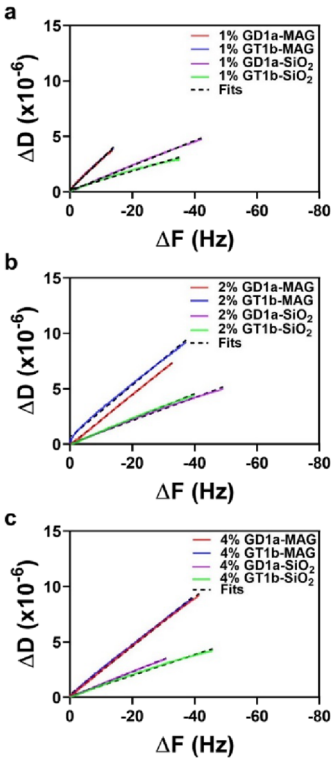

Figure 6. Dissipation shift as a function of frequency shift for vesicles binding to MAG-conjugated SLBs. ΔD vs ΔF plots for (a) 1%, (b) 2%, and (c) 4% GD1a and GT1b vesicles binding to MAG-conjugated SLBs and adsorption on SiO_2 surfaces.

Comparing the results in Figures 5 and 6 shows that the vesicle adsorption rate increases as a function of ganglioside mole fraction, but there is no significant difference in the vesicle deformation. The increase in adsorption rate can be explained by the higher probability of vesicle−MAG binding for each vesicle-surface encounter; however, once a vesicle is bound, the extent to which it is deformed is independent of the ganglioside mole fraction. Interestingly, measurements with giant vesicles have shown that bending rigidity for POPC membranes decreases as the mole fraction of GM1 ganglioside increases.[36] This coupled with the notion that increased number of ganglioside−MAG contacts would increase the adhesion strength, one would expect that vesicles with higher concentrations of gangliosides would deform more. However, this is not observed in our system, perhaps because MAG surface density, which is constant in our experiments, is the limiting factor in causing vesicle deformation. MAG regulates myelin−axon adhesion in concert with other proteins, including contactin-associated protein (Caspr), contactin 1, and neurofascin.[37−39] A recently developed model of axon myelination suggests that MAG−ganglioside interactions are important for maintaining a contact between the leading edge of myelin as it wraps around the axon.[6] If the membrane−membrane contacts governed by MAG−ganglioside interactions were too tight, this process might not proceed. Our results suggest membrane−membrane interactions governed by MAG−ganglioside binding are strong enough to hold the membranes together, but not strong enough to radically deform the membranes, which is consistent with this model of myelination.

Antiganglioside Antibodies Modulate MAG−Ganglioside Interactions by Competitive Inhibition. Antibodies against GD1a and GT1b can block MAG's ability to inhibit neurite outgrowth.[10] In addition, IgM antibodies that bind GD1a and GT1b can promote neurite extension[40,41] and block the ability of myelin to inhibit neurite outgrowth.[42] It has been suggested that the IgMs cluster gangliosides in lipid rafts and bring together signaling complexes that promote rather than inhibit neuronal growth.[41] Furthermore, the presence of pathogenic antibodies against gangliosides are among the hallmarks of Guillain−Barré syndrome,[43] an autoimmune disorder of the peripheral nervous system that results in dysfunction at the myelin−axon interface.[44] Here, using our SLB−vesicle binding approach, we investigated how antiganglioside antibodies can inhibit the ganglioside−MAG interactions. We first characterized the binding of antiganglioside antibodies to SLBs containing GD1a or GT1b. These antibodies (GD1a-1 and GT1b-2b) were initially developed by Schnaar and co-workers, and we use the same antibody

https://dx.doi.org/10.1021/acs.analchem.0c04412
Anal. Chem. XXXX, XXX, XXX−XXX

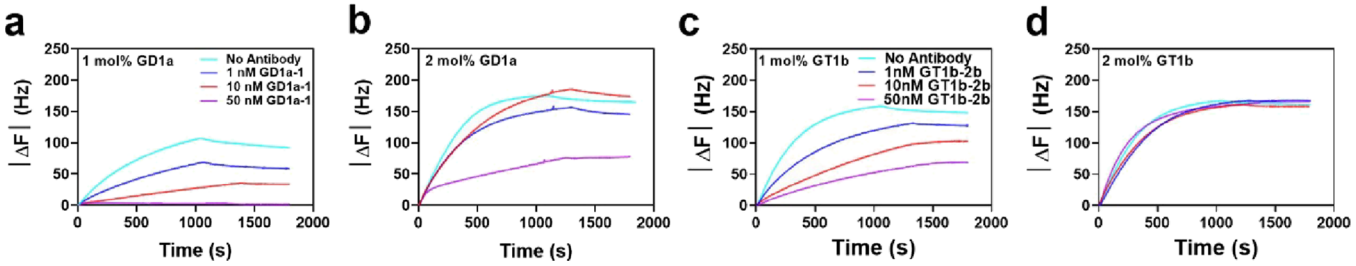

Figure 7. Ganglioside antibodies inhibit MAG binding. Inhibition of the binding of vesicles containing (a) 1% and (b) 2% GD1a to MAG by GD1a-1 antibody. Inhibition of the binding of vesicles containing (c) 1% and (d) 2% GT1b to MAG by GT1b-2b antibody.

nomenclature.[45] We determined the dissociation constants for GD1a-1 and GT1b-2b binding to SLBs with 1 and 2% GD1a and GT1b (Figure S9), respectively. For GD1a-1 binding to 1 and 2% GD1a SLBs, we determined a K_D of $(9.67 \pm 1.80) \times 10^{-11}$ M and $(1.58 \pm 0.20) \times 10^{-11}$ M, respectively. For GT1b-2b binding to 1 and 2% GT1b SLBs, the K_D values were $(3.11 \pm 2.61) \times 10^{-8}$ M and $(3.55 \pm 2.50) \times 10^{-8}$ M, respectively. This agrees with prior results showing that GD1a-1 is a stronger binder of GD1a than GT1b-2b is of GT1b.[45] Given the difference in ganglioside affinities of these two antibodies, we predicted that GD1a-1 would be a more potent inhibitor of GD1a−MAG interactions than GT1b-2b would be for GT1b-MAG interactions.

For MAG−ganglioside binding inhibition experiments, SLBs composed of POPC and 1% DGS-NTA were formed on the QCM-D sensor and functionalized with MAG as described above. The surface density of MAG on the SLB was held constant at an average frequency shift of −30 Hz, as in previous experiments. Vesicles (0.1 mg/mL total lipid) with 1 and 2% ganglioside were exposed to monoclonal antibodies ranging in concentration from 1 to 50 nM prior to injection into the QCM-D. In the presence of GD1a-1 antibody, the binding of vesicles with 1% GD1a to MAG was inhibited in a concentration-dependent fashion, with 50 nM GD1a-1 completely inhibiting binding (Figure 7a). When the vesicular concentration of GD1a is raised by 2%, the MAG binding inhibition is reduced due to the increased availability of GD1a on the vesicle surface (Figure 7b). Control experiments show that GD1a-1 does not bind MAG (Figure S10); therefore, the inhibition of vesicle binding can be attributed solely to GD1a-1 binding GD1a on vesicles.

With 1% GT1b vesicles, the GT1b-2b antibody inhibits binding to MAG in a concentration-dependent manner, but, at 50 nM, a significant vesicle binding is still observed (Figure 7c); thus, GT1b-2b is a weaker inhibitor of GT1b−MAG interactions compared to GD1a-1 inhibition of GD1a−MAG interactions. Control experiments showed that the GT1b-2b antibody does not bind MAG (Figure S10). Contrary to the case with GD1a vesicles and the GD1a-1 antibody, when the vesicular concentration of GT1b is 2%, the inhibition of MAG binding by GT1b-2b antibody is negligible (Figure 7d). The greater inhibition of GD1a−MAG binding by GD1a-1 compared to GT1b-2b inhibition of GT1b−MAG binding is due to the higher affinity of GD1a-1 for GD1a. The K_D for GD1a-1 binding to GD1a is roughly three orders of magnitude smaller. In neurite outgrowth assays, an antibody against GD1a was a more powerful blocker of MAG-mediated neurite outgrowth inhibition than was an antibody against GT1b.[10] While the exact identity of the antibodies was not specified, we assume them to be very similar to GD1a-1 and GT1b-2b since the same research group developed these antibodies. Taken together, these results show that monoclonal antibodies against GD1a and GT1b can inhibit ganglioside−MAG binding, and it is likely that this binding inhibition is responsible for the ability of antiganglioside antibodies to block the inhibition of neuronal outgrowth caused by myelin and MAG.

CONCLUSIONS

We demonstrate the development of a biosensor platform to detect, in real time, the binding of gangliosides on lipid bilayer vesicles to MAG conjugated to an SLB membrane. Our system, where both gangliosides and MAG are associated with fluid lipid bilayer membranes, is a realistic mimic of the interface between myelin and axons in the nervous system. This approach offers a level of control over the surface presentation and concentration of the gangliosides and MAG that can exceed that of traditional assays of binding between two membrane-associated species. Furthermore, the use of a QCM-D biosensor allows the determination of ganglioside−MAG binding constants, which have not been measured to date. The binding of ganglioside vesicles to MAG on SLBs is a multivalent interaction, much the same way that the interaction between the myelin and axon membranes involves multiple MAG−ganglioside contacts. Multivalent ligand−receptor interactions between surface-bound molecules can display unique properties like a superselectivity that is governed by the interplay between ligand and receptor surface coverage, mobility, and binding strength.[27,46] Through the use of vesicles and supported lipid bilayers, these properties in the context of myelination could be probed in a systematic fashion using a system where the diffusional mobility of ligands and receptors could be controlled by variation of the lipid composition and/or the experimental temperature. The binding of gangliosides by a number of toxins has been investigated in depth, and emerging evidence shows other components of the lipid membrane, particularly cholesterol, can modulate ganglioside structure and toxin binding properties.[47,48] The combination of ganglioside-rich vesicles and SLB-conjugated proteins could be used to probe how various agents, such as membrane cholesterol, can modulate endogenous glycolipid−protein interactions using either the QCM-D approach described here or other detection techniques like total internal reflection fluorescence microscopy.[49−51]

ASSOCIATED CONTENT

Supporting Information

The Supporting Information is available free of charge at https://pubs.acs.org/doi/10.1021/acs.analchem.0c04412.

https://dx.doi.org/10.1021/acs.analchem.0c04412
Anal. Chem. XXXX, XXX, XXX−XXX

BSA injection over SLB; stability of MAG conjugation to the SLB; FRAP analysis of SLBs before and after MAG conjugation; FRAP recovery curves; lipid diffusion coefficients; vesicle sizes and zeta potential measurements; dissipation shift for GD1a and GT1b vesicles binding to MAG-conjugated SLBs; ganglioside vesicles containing 1% GD1a and 1% GT1b do not bind POPC/DGS-NTA membranes; vesicles lacking gangliosides and vesicles containing GM1 or GD1b do not bind MAG-conjugated SLBs; summary of kinetic data; antibody binding to SLBs with GD1a and GT1b; and antiganglioside antibodies GD1a-1 and GT1b-2b do not bind MAG (PDF)

AUTHOR INFORMATION

Corresponding Author

Nathan J. Wittenberg − *Department of Chemistry, Lehigh University, Bethlehem, Pennsylvania 18015, United States;* orcid.org/0000-0001-9196-1867; Email: njw@lehigh.edu

Authors

Jennie L. Cawley − *Department of Chemistry, Lehigh University, Bethlehem, Pennsylvania 18015, United States*

Luke R. Jordan − *Department of Chemistry, Lehigh University, Bethlehem, Pennsylvania 18015, United States*

Complete contact information is available at: https://pubs.acs.org/10.1021/acs.analchem.0c04412

Author Contributions

J.L.C., L.R.J., and N.J.W. designed experiments, J.L.C. carried out the experiments, J.L.C and N.J.W. analyzed the data, and J.L.C and N.J.W. wrote the manuscript.

Notes

The authors declare no competing financial interest.

ACKNOWLEDGMENTS

The authors acknowledge funding from Lehigh University and the National Institutes of Health (R21GM134414). The authors also acknowledge Viola Yu for creating illustrations. The monoclonal antibodies were obtained from the Developmental Studies Hybridoma Bank, created by NICHD of the NIH and maintained at The University of Iowa, Department of Biology, Iowa City, IA, USA.

REFERENCES

(1) Snaidero, N.; Mobius, W.; Czopka, T.; Hekking, L. H.; Mathisen, C.; Verkleij, D.; Goebbels, S.; Edgar, J.; Merkler, D.; Lyons, D. A.; Nave, K. A.; Simons, M. *Cell* **2014**, *156*, 277−290.

(2) Yiu, G.; He, Z. *Nat. Rev. Neurosci.* **2006**, *7*, 617−627.

(3) Crocker, P. R.; Paulson, J. C.; Varki, A. *Nat. Rev. Immunol.* **2007**, *7*, 255−266.

(4) Schnaar, R. L.; Lopez, P. H. H. *J. Neurosci. Res.* **2009**, *87*, 3267−3276.

(5) Pronker, M. F.; Lemstra, S.; Snijder, J.; Heck, A. J.; Thies-Weesie, D. M.; Pasterkamp, R. J.; Janssen, B. J. *Nat. Commun.* **2016**, *7*, 13584.

(6) Djannatian, M.; Timmler, S.; Arends, M.; Luckner, M.; Weil, M. T.; Alexopoulos, I.; Snaidero, N.; Schmid, B.; Misgeld, T.; Mobius, W.; Schifferer, M.; Peles, E.; Simons, M. *Nat. Commun.* **2019**, *10*, 4794.

(7) Kelm, S.; Pelz, A.; Schauer, R.; Filbin, M. T.; Tang, S.; de Bellard, M. E.; Schnaar, R. L.; Mahoney, J. A.; Hartnell, A.; Bradfield, P.; et al. *Curr. Biol.* **1994**, *4*, 965−972.

(8) Mehta, N. R.; Lopez, P. H. H.; Vyas, A. A.; Schnaar, R. L. *J. Biol. Chem.* **2007**, *282*, 27875−27886.

(9) Filbin, M. T. *Nat. Rev. Neurosci.* **2003**, *4*, 703−713.

(10) Vyas, A. A.; Patel, H. V.; Fromholt, S. E.; Heffer-Lauc, M.; Vyas, K. A.; Dang, J.; Schachner, M.; Schnaar, R. L. *Proc. Natl. Acad. Sci. U. S. A.* **2002**, *99*, 8412−8417.

(11) Vyas, A. A.; Blixt, O.; Paulson, J. C.; Schnaar, R. L. *J. Biol. Chem.* **2005**, *280*, 16305−16310.

(12) Mountney, A.; Zahner, M. R.; Lorenzini, I.; Oudega, M.; Schramm, L. P.; Schnaar, R. L. *Proc. Natl. Acad. Sci. U. S. A.* **2010**, *107*, 11561−11566.

(13) Collins, B. E.; Yang, L. J.-S.; Mukhopadhyay, G.; Filbin, M. T.; Kiso, M.; Hasegawa, A.; Schnaar, R. L. *J. Biol. Chem.* **1997**, *272*, 1248−1255.

(14) Vinson, M.; Strijbos, P. J. L. M.; Rowles, A.; Facci, L.; Moore, S. E.; Simmons, D. L.; Walsh, F. S. *J. Biol. Chem.* **2001**, *276*, 20280−20285.

(15) Reviakine, I.; Johannsmann, D.; Richter, R. P. *Anal. Chem.* **2011**, *83*, 8838−8848.

(16) Di Iorio, D.; Verheijden, M. L.; van der Vries, E.; Jonkheijm, P.; Huskens, J. *ACS Nano* **2019**, *13*, 3413−3423.

(17) Parveen, N.; Rydell, G. E.; Larson, G.; Hytonen, V. P.; Zhdanov, V. P.; Hook, F.; Block, S. *J. Am. Chem. Soc.* **2019**, *141*, 16303−16311.

(18) Hsia, C. Y.; Chen, L.; Singh, R. R.; DeLisa, M. P.; Daniel, S. *Sci. Rep.* **2016**, *6*, 32715.

(19) van der Meulen, S. A. J.; Dubacheva, G. V.; Dogterom, M.; Richter, R. P.; Leunissen, M. E. *Langmuir* **2014**, *30*, 6525−6533.

(20) Mensch, A. C.; Buchman, J. T.; Haynes, C. L.; Pedersen, J. A.; Hamers, R. J. *Langmuir* **2018**, *34*, 12369−12378.

(21) Kučerka, N.; Nieh, M.-P.; Katsaras, J. *Biochim. Biophys. Acta* **2011**, *1808*, 2761−2771.

(22) Jönsson, P.; Jonsson, M. P.; Tegenfeldt, J. O.; Höök, F. *Biophys. J.* **2008**, *95*, 5334−5348.

(23) Schindelin, J.; Arganda-Carreras, I.; Frise, E.; Kaynig, V.; Longair, M.; Pietzsch, T.; Preibisch, S.; Rueden, C.; Saalfeld, S.; Schmid, B.; Tinevez, J. Y.; White, D. J.; Hartenstein, V.; Eliceiri, K.; Tomancak, P.; Cardona, A. *Nat. Methods* **2012**, *9*, 676−682.

(24) Keller, C. A.; Kasemo, B. *Biophys. J.* **1998**, *75*, 1397−1402.

(25) Cho, N.-J.; Frank, C. W.; Kasemo, B.; Höök, F. *Nat. Protoc.* **2010**, *5*, 1096−1106.

(26) Ma, G. J.; Ferhan, A. R.; Jackman, J. A.; Cho, N.-J. *Commun. Mater.* **2020**, *1*, 45.

(27) Martinez-Veracoechea, F. J.; Frenkel, D. *Proc. Natl. Acad. Sci. U. S. A.* **2011**, *108*, 10963−10968.

(28) Duarte, A. A.; Filipe, S. L.; Abegao, L. M.; Gomes, P. J.; Ribeiro, P. A.; Raposo, M. *Microsc. Microanal.* **2013**, *19*, 867−875.

(29) Poirier, C.; van Effenterre, D.; Delord, B.; Johannes, L.; Roux, D. *Biochim. Biophys. Acta* **2008**, *1778*, 2450−2457.

(30) Seifert, U. *Adv. Phys.* **1997**, *46*, 13−137.

(31) Reviakine, I.; Gallego, M.; Johannsmann, D.; Tellechea, E. *J. Chem. Phys.* **2012**, *136*, No. 084702.

(32) Seifert, U.; Lipowsky, R. *Phys. Rev. A* **1990**, *42*, 4768−4771.

(33) Reimhult, E.; Höök, F.; Kasemo, B. *Langmuir* **2003**, *19*, 1681−1691.

(34) Rydell, G. E.; Dahlin, A. B.; Hook, F.; Larson, G. *Glycobiology* **2009**, *19*, 1176−1184.

(35) Jordan, L. R.; Blauch, M. E.; Baxter, A. M.; Cawley, J. L.; Wittenberg, N. J. *Colloids Surf., B* **2019**, *183*, 110442.

(36) Fricke, N.; Dimova, R. *Biophys. J.* **2016**, *111*, 1935−1945.

(37) Montag, D.; Giese, K. P.; Bartsch, U.; Martini, R.; Lang, Y.; Bluthmann, H.; Karthigasan, J.; Kirschner, D. A.; Wintergerst, E. S.; Nave, K. A.; et al. *Neuron* **1994**, *13*, 229−246.

(38) Rios, J. C.; Melendez-Vasquez, C. V.; Einheber, S.; Lustig, M.; Grumet, M.; Hemperly, J.; Peles, E.; Salzer, J. L. *J. Neurosci.* **2000**, *20*, 8354−8364.

(39) Charles, P.; Tait, S.; Faivre-Sarrailh, C.; Barbin, G.; Gunn-Moore, F.; Denisenko-Nehrbass, N.; Guennoc, A. M.; Girault, J. A.; Brophy, P. J.; Lubetzki, C. *Curr. Biol.* **2002**, *12*, 217−220.

https://dx.doi.org/10.1021/acs.analchem.0c04412
Anal. Chem. XXXX, XXX, XXX−XXX

(40) Xu, X.; Warrington, A. E.; Wright, B. R.; Bieber, A. J.; Van Keulen, V.; Pease, L. R.; Rodriguez, M. *J. Neurochem.* **2011**, *119*, 100−112.
(41) Xu, X.; Denic, A.; Jordan, L. R.; Wittenberg, N. J.; Warrington, A. E.; Wootla, B.; Papke, L. M.; Zoecklein, L. J.; Yoo, D.; Shaver, J.; Oh, S. H.; Pease, L. R.; Rodriguez, M. *Dis. Model Mech.* **2015**, *8*, 831−842.
(42) Warrington, A. E.; Bieber, A. J.; Van Keulen, V.; Ciric, B.; Pease, L. R.; Rodriguez, M. *J. Neuropathol. Exp. Neurol.* **2004**, *63*, 461−473.
(43) Kaida, K.; Ariga, T.; Yu, R. K. *Glycobiology* **2009**, *19*, 676−692.
(44) He, L.; Zhang, G.; Liu, W.; Gao, T.; Sheikh, K. A. *J. Neurosci.* **2015**, *35*, 6770−6785.
(45) Schnaar, R. L.; Fromholt, S. E.; Gong, Y.; Vyas, A. A.; Laroy, W.; Wayman, D. M.; Heffer-Lauc, M.; Ito, H.; Ishida, H.; Kiso, M.; Griffin, J. W.; Shiekh, K. A. *Anal. Biochem.* **2002**, *302*, 276−284.
(46) Dubacheva, G. V.; Araya-Callis, C.; Geert Volbeda, A.; Fairhead, M.; Codee, J.; Howarth, M.; Richter, R. P. *J. Am. Chem. Soc.* **2017**, *139*, 4157−4167.
(47) Mahfoud, R.; Manis, A.; Binnington, B.; Ackerley, C.; Lingwood, C. A. *J. Biol. Chem.* **2010**, *285*, 36049−36059.
(48) Lingwood, D.; Binnington, B.; Rog, T.; Vattulainen, I.; Grzybek, M.; Coskun, U.; Lingwood, C. A.; Simons, K. *Nat. Chem. Biol.* **2011**, *7*, 260−262.
(49) Gunnarsson, A.; Dexlin, L.; Wallin, P.; Svedhem, S.; Jonsson, P.; Wingren, C.; Hook, F. *J. Am. Chem. Soc.* **2011**, *133*, 14852−14855.
(50) Lee, D. W.; Hsu, H. L.; Bacon, K. B.; Daniel, S. *PLoS One* **2016**, *11*, e0163437.
(51) Kunze, A.; Bally, M.; Höök, F.; Larson, G. *Sci. Rep.* **2013**, *3*, 1452.

https://dx.doi.org/10.1021/acs.analchem.0c04412
Anal. Chem. XXXX, XXX, XXX−XXX